# Development of laser speckle blood flowmeter for evaluating the physiological function of skin

# Development of laser speckle blood flowmeter for evaluating the physiological function of skin

**Yoshinao Nagashima[1,2,3], Yuko Ohsugi[1,2], Makiko Hiraishi[1], Yoshifumi Niki[1], Akira Fuji[1], Masataka Majima[2], and Takashi Okamoto[3]**

[1]Personal Health Care Products Research Laboratories, Kao Corporation, Tokyo, Japan, 131-8501
[2]Department of Pharmacology, Kitasato University School of Medicine, Kanagawa, Japan, 252-0374
[3]Department of Physics and Information Technology, Kyushu Institute of Technology, Fukuoka, Japan, 820-8502

Yoshinao Nagashima**,** E-mail: nagashima.yoshinao@kao.com

## Abstract

*Objective*: We developed and demonstrated laser speckle flowgraphy (LSFG) for two-dimensional (2D) skin blood flow (SBF) measurements to facilitate the noninvasive comparisons of SBF between individuals. *Approach*: By using morphing technology with a face mesh to compare SBF spatial distributions among individuals, we examined the practicability of SBF measurement with LSFG. *Main results*: (1) The uniformity of SBF measurement was demonstrated by examinations at different distances and angles for healthy subjects. (2) Mean blur rate (MBR)—a blood flow index of LSFG—exhibited significant correlation with the thermal diffusion method (TDM)—an established blood flow measurement method—suggesting that MBR is an effective index of SBF. (3) Blowout time, the half-width duration/duration of one cardiac cycle, exhibited significant negative correlation with age and positive correlation with stratum corneum hydration. *Significance*: These results suggest that LSFG is useful for evaluating SBF-related skin properties, and it has significant potential in medicine and cosmetology.

Keywords: skin blood flow, laser speckle flowgraphy, strain-gauge plethysmography, aging, stratum corneum hydration, morphing, thermal diffusion.

## 1. Introduction

Internal and external environmental factors such as stress and fatigue may adversely affect the physiological function of skin by limiting its hemodynamic response. To improve these physiological situations, skin hemodynamic properties in individuals at multiple occasions should be evaluated accurately. We previously developed an integration-type laser Doppler flowmeter with a temperature-loading instrument[1] as an improved version of a previously reported device[2-4]. Recently, several devices have been developed for the 2D visualization of skin blood flow (SBF)[5,6]. Fujii et al. developed a widely used laser-speckle-based device to measure retinal blood flow[7]. Although laser light is known to irradiate the ocular fundus, when measuring the SBF in the entire face, this device diffuses laser light over the entire face and the irradiated energy per unit area of the face is sufficiently low; thus, this approach is safe. Therefore, we further improved the previously reported laser speckle blood flowmeter for the measurement of facial SBF.

## 2. Materials and Methods

### 2.1 Laser Speckle Blood Flowmeter

#### 2.1.1 Device configuration

Laser speckle flowgraphy (LSFG) comprises a probe unit that has a laser module with 830-nm wavelength, color CMOS camera with 640 × 480 pixel resolution, and monochrome

Author *et al*

CCD camera with $600 \times 480$ pixel resolution; this probe emits class 1M laser light according to the IEC 60825-1 standard. The LSFG also comprises a control unit that controls the laser output and CCD camera of the probe and a PC equipped with the measurement and analysis software. A probe unit for animal experiments, control unit, and PC (LSFG-ANW, Softcare Co., Ltd., Fukuoka, Japan) were employed to develop a prototype for this trial. The hardware electric noises are not corrected. However, as a result, stable blood flow results have been achieved. LSFG is a blood flow distribution imaging system developed by Fujii Laboratory, Kyushu Institute of Technology[8].

### 2.1.2 LSFG measurement principle

Figure 1(a) shows that using the 830-nm coherent laser light source, the speckle pattern of irradiated particles changes shape according to the motion of each particle. When erythrocytes in blood vessels are irradiated with laser light, they move in the blood vessels while changing positional relationships. Thus, their speckle pattern changes constantly and randomly. The measurement principle of LSFG is to calculate the blood flow through a statistical analysis of the fluctuation of the speckle pattern[8]. Figure 1(b) shows a mapping image in which the blood flow image is superimposed onto the facial image. Figure 1(c) shows an LSFG system.
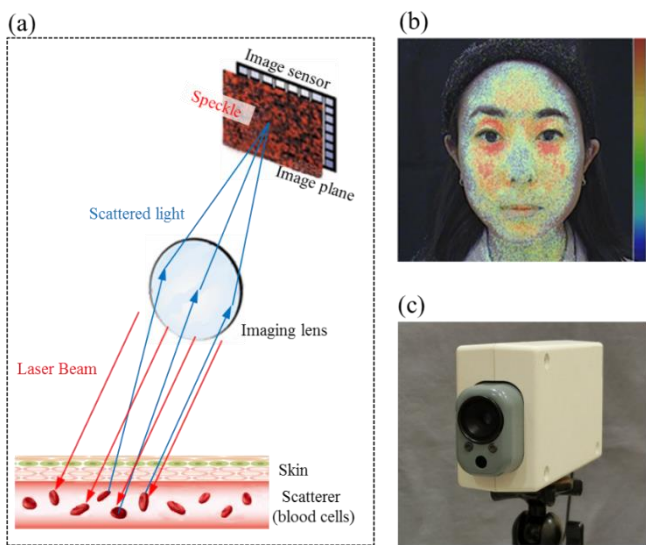


**Figure 1** Principle and outline of LSFG.
(a) Principle of LSFG: A laser irradiates the skin through the LSFG blood flow measurement device (c), and a random speckle pattern of reflected scattered light created by erythrocytes in the blood vessels is detected by the image sensor. (b) mapping images (blood flow image is superimposed onto facial image); and (c) the laser speckle blood flowmeter under development (LSFG).

The speckle imaged with a lens is detected using an image sensor. The output value of each pixel of the detector equals the light intensity integrated by the exposure time (shutter speed) $\Delta T$ of the detector. When the average light intensity of the speckle image received by pixel $k$ at time $t$ is $i_k(t)$, the light intensity $I_k(n)$ received by pixel $k$ of the detector in the $n$th frame is given by[8]

$$I_k(n) = \int_n^{n+\Delta T} i_k(t)\, dt. \tag{1}$$

### 2.1.3 Blood flow index of LSFG

The mean blur rate (MBR), which is an index of tissue blood flow used in LSFG, is calculated from the spatial and temporal blur rate of a speckle pattern. For example, when we take a photo of a moving object, we find that the image is blurred. When describing the blur rate of a spatially varying speckle pattern using contrast, we find an inverse relationship between the velocity and the contrast of the object. $MBR_{n,m,t}$ denotes the MBR of the $(n, m)$th pixel point at time $t$, and the $I_{n,m,t}$ values indicate the output intensity of speckle images at the calculated MBR pixel point. In addition, $\langle I_{n,m,t}\rangle$ is the mean intensity of the surrounding pixel points in the temporal and spatial directions, including the calculated MBR pixel point. $MBR_{n,m,t}$ is calculated as[7]

$$MBR_{n,m,t} = \frac{\langle I_{n,m,t}\rangle^2}{\langle |I_{n,m,t} - \langle I_{n,m,t}\rangle|\rangle^2}. \tag{2}$$

Figure 2 shows the modeling of the time-varying blur rate of the speckle pattern on an image sensor. The horizontal axis denotes the measurement time and the vertical axis denotes the variation in the light intensity of the speckle pattern, which reflects the motion of the measured object. The blue solid line in the figure denotes the output from the image sensor. In Fig. 2(a), it is assumed that erythrocytes move gradually. The image obtained using the image sensor shows the slow motion of the erythrocytes. In other words, because the speckle pattern changes gradually, an image with high contrast and low MBR (i.e., low SBF) is obtained; in contrast, in Fig. 2(b), it is assumed that erythrocytes move rapidly. The image obtained using the image sensor shows the rapid motion of the erythrocytes. In other words, because the speckle pattern changes rapidly, an image with low contrast and high MBR (i.e., high SBF) is obtained. Thus, the MBR is directly proportional to the erythrocyte velocity and is inversely proportional to the square of the speckle light intensity contrast[11].
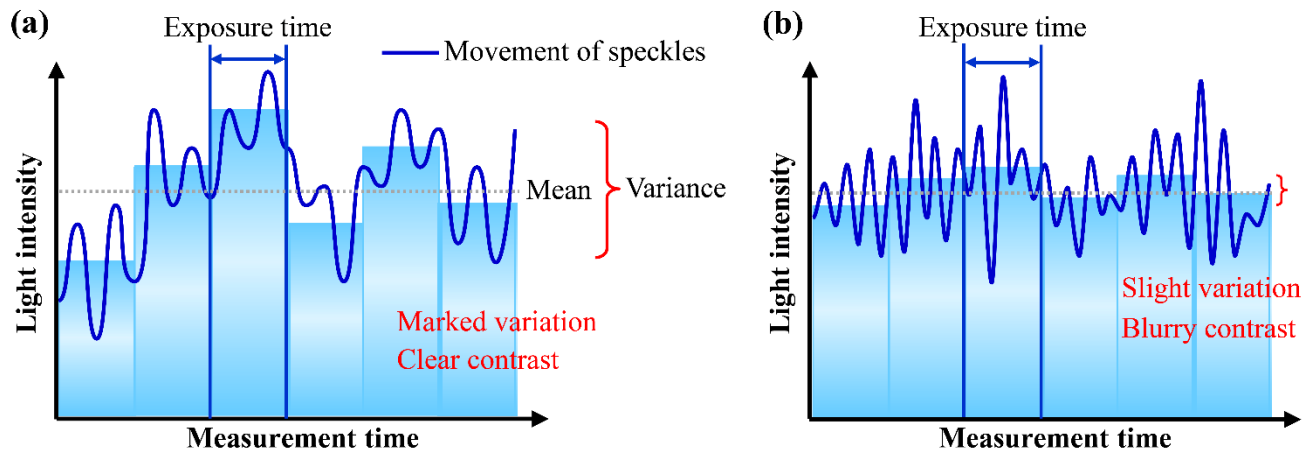
**Figure 2** Calculation of MBR, which is an index of SBF.

MBR is an index of SBF and is calculated as the inverse of the square of the contrast in light intensity detected by the image sensor. (a) When erythrocyte velocity is low, the image is less blurred, thereby reducing the MBR (low SBF); and (b) when erythrocyte velocity is high, the image is more blurred, thereby increasing the MBR (high SBF).

### 2.1.4 How to analyze LSFG

Figure 3 shows how to analyze LSFG. A frame (fully rendered image of the entire image) is divided into two fields (partial images acquired by each scan). In the first field, odd-numbered lines are horizontally scanned in 1/60 s. In the second field, even-numbered lines are horizontally scanned in 1/60 s. Then, the first and second fields are synthesized at 30 frames/s (2:1 interlace). The light intensity map (speckle images) shown in Fig. 3(a) comprises data obtained using the LSFG equipment, representing laser light intensity. A blood flow map (MBR image) was created by calculating the MBR of the speckle pattern from three frames of light intensity maps. The next frame of the blood flow map was determined from the next three frames of the light intensity map shifted by one frame (blood flow map of the $(N - 2)^{th}$ frame was generated based on the light intensity map of the $N^{th}$ frame). The heart rate detected from continuous waveform data in the blood flow map was averaged to a single heartbeat for each frame and summarized as a heartbeat map (an image in which the blood flow map is normalized with a heartbeat). Each area was averaged based on the heartbeat cycles that were automatically detected by the analysis software. The heartbeat map has less noise than the blood flow map. A composite map (mean blood flow image) is a frame of a still image in which all frames of the heartbeat maps are averaged (when a heartbeat map is not created, all frames of blood flow maps are averaged). Thus, a sharp, low-noise image can be obtained. The mapping image (obtained by superimposing the blood flow image onto the facial image) shown in Fig. 3(b) was created by superimposing the heartbeat map image (i.e., composite map) onto the video image based on the corresponding points (e.g., outer canthus point, inner canthus point, subnasal point, and corners of mouth). The transparency of the heartbeat map image and the video image in Fig. 3(c) can be adjusted arbitrarily. This study used a mapping image in which the video image and heartbeat map image were 60% blended. In the mapping image, boundaries between each facial area, which cannot be observed with the heartbeat map alone, become clear.

### 2.1.5 About the parameters of the optical system

Measurements were taken under the following conditions by modifying LSFG-ANW.

The distance between the minimum aperture of the imaging system and the image sensor is an important factor that determines speckle size. To focus on two measurement distances (50 and 25 cm), the distance between the imaging lens of focal distance 12 mm and the imaging sensor were displaced. The distance between the principal point and the image sensors at the two measurement distances of 50 and 25 cm were approximately 12.3 and 12.6 mm, respectively, exhibiting a slight variation of 1%, which has a negligible effect on speckle size. The aperture was set such that the speckle size was similar to the CCD camera cell size. The moment of the speckle pattern can be captured by increasing shutter speed (i.e., shortening exposure time). However, this weakens the signal, increasing the laser power. Conversely, the laser power can be decreased by slowing the shutter speed (i.e., prolonging exposure time). However, this lowers the effective time resolution and linearity with MBR in high-speed regions. We considered the findings of Konishi et al. (ref 7) that a larger spatial window size used to calculate MBR decreases noise by smoothing, however, conversely decreases blood flow response.
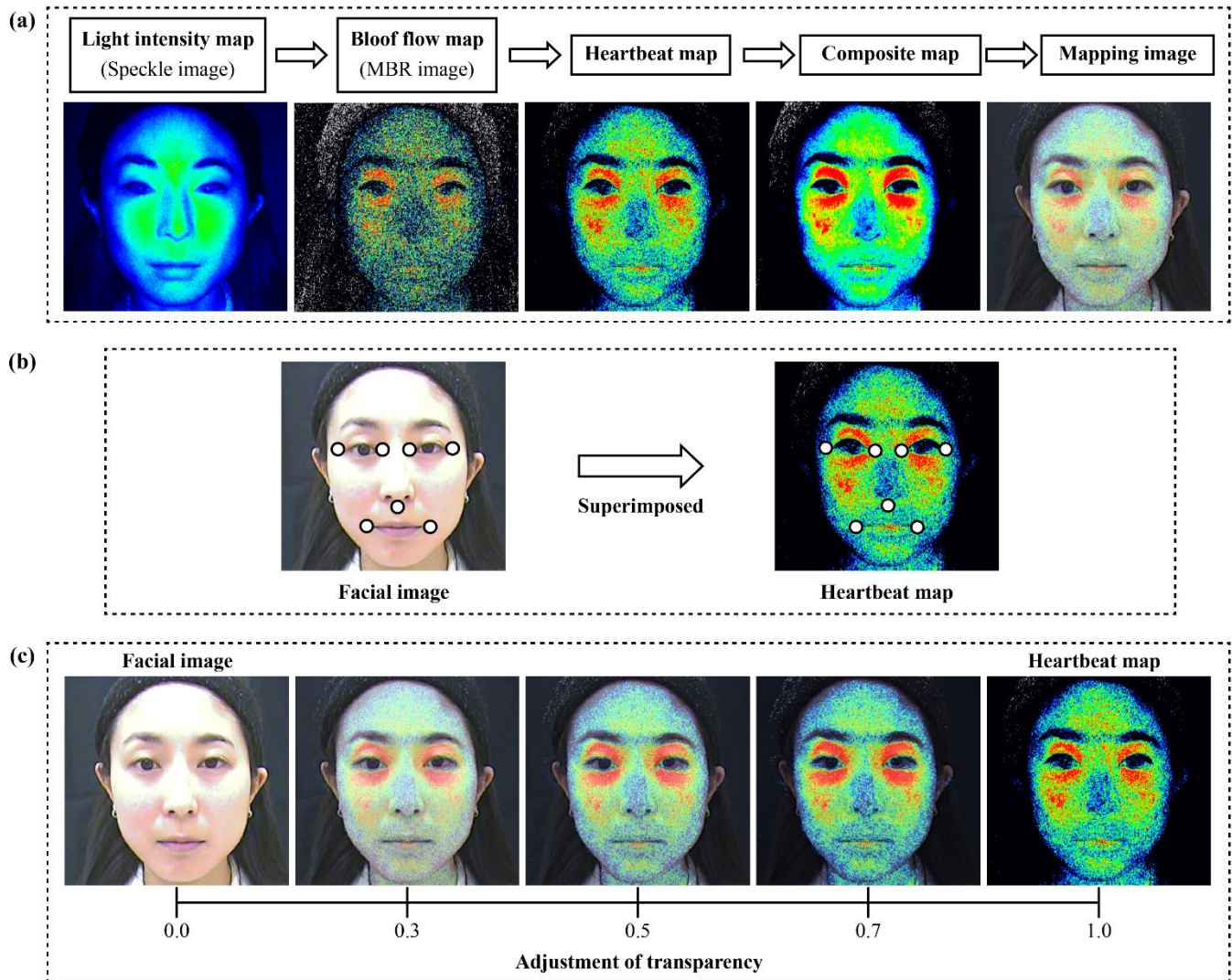
**Figure 3** Analysis of data from LSFG.
(a) Light intensity map: data measured by LSFG; blood flow map: it can be calculated by processing the light intensity map; heartbeat map: it can be calculated by averaging the blood flow map values into a single heartbeat; composite map: a map that averages all frames of the heartbeat map; and mapping images: mapping of a heartbeat map and a video image; (b) the blood flow image was superimposed onto the facial image using corresponding points; and (c) the transparency of the heartbeat map and video image was adjusted.

### 2.1.6 Face coordinates

Figure 4 shows the morphing technology with the face mesh as a method to compare localized differences in facial SBF among individuals[10,11]. The number of facial feature points for detecting the face area was set to 70 (i.e., 22 points around the eyes, 10 points for the eyebrows, 9 points around the nose, 14 points around the mouth, 4 points for the nasolabial groove, and 11 points for the facial contour). The facial feature points (Fig. 4(b)) were extracted based on artificial intelligence using facial feature detection software

(FaceSDK 6.2., Luxand, Maryland, USA) to create a face mesh (42 × 42) (Fig. 4(c)) automatically. For fine adjustment of the face mesh, the lattice points were adjusted using a mouse. The 177,241 intersection points that divide the x, y coordinates of the lattice points into 10 equal lattice points were used as sublattice points. The sublattice points were provided to the x-coordinates, y-coordinates, and MBR, and a 32-bit true color corresponding to the MBR of the mapping image Fig. 4(d). Figure 4(e) shows that by selecting an area in the mapping image, the blood flow in the facial region of interest (ROI) can be calculated in proportion to the face size.
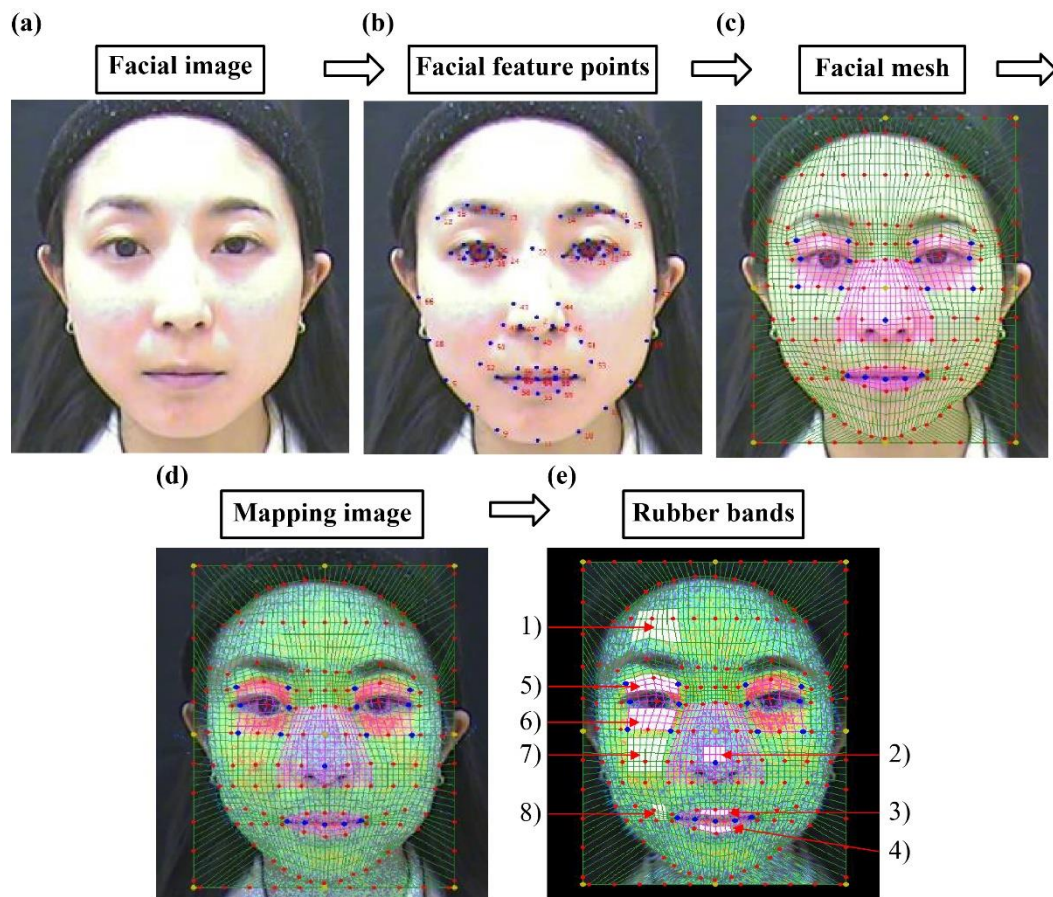
Author *et al*



**Figure 4** Setting of the site of SBF measurement with a face mesh.
(a) The face area is detected from the facial image; (b) facial feature points are obtained using artificial intelligence automatically; (c) a face mesh is created from the mapping image; (d) by selecting ROIs (e) to set the locations of SBF measurement: 1) forehead, 2) nasal tip, 3) upper lip, 4) lower lip, 5) upper eyelid, 6) lower eyelid, 7) cheek, and 8) corners of mouth.

### 2.2 How to Create Mapping Images with LSFG

Our custom analysis software, a modified version of the software for LSFG-ANW (LSFG Analyzer), was used to identify the cycles of the heartbeat based on the blood flow waveform of the analyzed site and to detect the dips to measure the heart rate to create the heartbeat map image from the continuous waveforms of the blood flow map image. An electrocardiography (ECG) limb lead II was recorded simultaneously with LSFG. A peak blood flow waveform is observed with a delay from the R-wave on ECG. Tamaki et al. demonstrated that the waveform of optic disc and choroid blood flow recorded by LSFG exhibited periodic variations synchronous with the ECG waveforms[12]. By using an image processing software (LSFG Movie Maker), the color video and heartbeat map images were then superimposed to create a mapping image in which the color video and heartbeat map images were 60% blended. From the mapping image, MBR was calculated as a blood flow index.

### 2.3 Effect of Surface Reflection Light Reduction by Placing a Polarizing Filter

In general, laser light irradiated on the skin is recorded using the probe unit (Fig. 1(c)) with specularly reflected light and light scattered by blood cells in subcutaneous vessels added. Of these, the former increases owing to excess sebum, sweat, deep wrinkles, and severe irritation. Furthermore, because it is reflected on the skin surface, it does not contain blood flow information and increases the noise component called static scatter. Thus, a linear polarizer that passes light with a polarization direction perpendicular to that of the surface-reflected light was placed in front of the probe unit (Fig. 1 (c)) to eliminate the surface reflected light[13-15].

### 2.4 Comparison of Uniformity of SBF Measured at Different Distances

Conventional laser speckle blood flowmeters measure blood flow at a constant distance. However, uniform measurement across different distances is required for

comparing SBF in the entire face and that in small areas of the face. Using the test machine, we investigated the degree of stability by performing comparative measurements of SBF on the same site at two distances: 50 cm (measures SBF of the entire face); considering the laser power, CCD camera sensitivity, and distortion optics, and at 25 cm (measures SBF of the face in more detail); capturing measurement areas in approximately one-fourth of the entire face.

### 2.4.1 Participants and measurement conditions

A total of 60 healthy females in their 20s and 30s (28.3 ± 3.53 years of age) were included in this study. They were habituated for 30 min in the semi-supine posture at room temperature and humidity of 25 °C and 50% RH, respectively. For the LSFG measurement, SBF was measured from the front with the head fixed and right cheek at a distance of 25 and 50 cm from the probe unit. The order of short-distance (i.e., 25 cm) and long-distance (i.e., 50 cm) measurements was randomized. Continuous measurement (30 frames/s, 2:1 interlace) at one distance was performed for 30 s. Immediately afterward, a 30-s measurement was performed at another distance. Motion artifacts were minimized by limiting body movement as much as possible by fixing the head and forearms with participants in the semi-supine position.

### 2.4.2 Analysis

A mapping image was created according to the method described in Section 2.2. The analysis site was the right cheek (1.5 × 1.5 cm). From the mapping image obtained during a 30-s measurement, MBR was calculated as a blood flow index.

### 2.5 Comparison of Uniformity of SBF Measured at Different Angles

Conventional laser speckle blood flowmeters measure blood flow at a constant angle. However, when measuring the SBF of the entire face from the front (at an angle of 0°), the analysis of the SBF of the eye corners and cheek (outer side of cheek) along the face edge involves higher measurement errors than that of the forehead, nasal tip, jaw, eyelid, cheek (center side of cheek), lip, corners of mouth, etc. owing to the edge effect. Thus, we examined SBF measurement accuracy for measurement angles of −45° (left front) to 45° (right front).

### 2.5.1 Participants and measurement conditions

Five healthy females in their 20s and 50s (33.8 ± 10.3 years of age) were included in the pilot study in which SBF measurement was performed for measurement angles of −45° (left front) to 45° (right front). Sixty healthy females in their 20s and 30s (28.3 ± 3.53 years of age) were included in the main study in which SBF measurement was performed for measurement angles of −30° (left front) to 0° (front) and 0° (front) to 30° (right front). The subjects were habituated for 30 min in the semi-supine posture at 25 °C and 50% RH,

respectively. In the preliminary study, the blood flow measurement was performed at 5° intervals from −45° (left front) to −20° (left front), 10° intervals from −20° (left front) to 20° (right front), and 5° intervals from 20° (right front) to −45° (right front) with the head fixed and the forehead at 50-cm measurement distance from the probe unit. The measurement order was randomized (i.e., (1) from 0° (front) to −45° (left front) and (2) from 0° (front) to 45° (right front)), and four measurements were performed for each site. In the main study, the measurement order was randomized (i.e., (1) from 0° (front) to −30° (left front) and (2) from 0° (front) to 30° (right front)), and four measurements were performed for each site. The measurement (30 frames/s, 2:1 interlace) was recorded for 5 s for each measurement angle. Immediately afterward, another 5-s measurement was performed at another angle.

### 2.5.2 Analysis

A mapping image was created according to the method in Section 2.2. The analysis site was the forehead (0.9 × 1.8 cm). From the mapping image obtained during a 5-s measurement, MBR was calculated as a blood flow index.

### 2.6 Comparison Between TDM and LSFG

When SBF exceeds a certain level, skin temperature reaches a plateau, making it impossible to estimate the SBF[16]. The thermal diffusion method (TDM) focuses on the fact that skin thermal conductivity exhibits a linear relationship with SBF[17]. Sakai et al. developed a method to calculate tissue blood flow from the slope of the thermal clearance curve transiently[18]. To compare LSFG and SBF using this method, we developed a prototype system that allows noncontact 2D measurement of the SBF. A far-infrared heater was used for thermal loading and thermography was used for skin temperature measurement.

### 2.6.1 Theoretical formula of TDM

The thermal clearance curve can be approximated by the exponential, and Newton's law of cooling can be applied. Therefore, temperature T(t) of the electrode tip at an arbitrary time is given by

$$T = T_0 \exp(-\alpha k t) \tag{3}$$

where $T_0$: temperature peak value, $k$: thermal conductivity, $\alpha$: constant, $t$: time

$\alpha$ is calculated using a substance with a known thermal conductivity. According to Grayson's theory, skin thermal conductivity and SBF are proportional to each other (Grayson, 1952)[19]; thus, the skin thermal conductivity while blood is flowing is given by

$$K = K_0 + \beta F \tag{4}$$

where, $K$: thermal conductivity of skin tissue with blood flow, $K_0$: thermal conductivity of skin tissue without blood flow, $\beta$: transformation constant, and $F$: Skin blood flow.

As peak temperature varies with SBF, substitute equation (4) into equation (3) with $T_1$: skin temperature with blood flow and $T_2$: skin temperature without blood flow to obtain the equation of thermal clearance with blood flow as follows:

$$T_1(t) = T_1 \exp(-\alpha(K_0 + \beta F)t) \tag{5}$$

along with the equation of thermal clearance without blood flow

$$T_2(t) = T_2 \exp(-\alpha K_0 t) \tag{6}$$

The logarithm of both sides of equations (5) and (6) are identified as follows:

$$\log_e T_1(t) = \log_e T_1 - \alpha(K_0 + \beta F)t \tag{7}$$

$$\log_e T_2(t) = \log_e T_2 - \alpha K_0 t \tag{8}$$

To determine the slopes of equations (7) and (8), both sides of each equation should be differentiated by time $t$ to obtain

$$\frac{d\log_e T_1(t)}{dt} = -\alpha(K_0 + \beta F) \tag{9}$$

$$\frac{d\log_e T_2(t)}{dt} = -\alpha K_0 \tag{10}$$

According to equations (9) and (10), the difference of the slopes is

$$\frac{d\log_e T_1(t)}{dt} - \frac{d\log_e T_2(t)}{dt} = -\alpha\beta F \tag{11}$$

Therefore,

$$F = -\frac{1}{\alpha\beta}\left(\frac{d\log_e T_1(t)}{dt} - \frac{d\log_e T_2(t)}{dt}\right) \tag{12}$$

This equation indicates that SBF is proportional to the slope of the thermal clearance curve. However, this method requires $T_2$ to be measured (i.e., skin temperature when blood is not flowing). In limb measurement, $T_2$ can be measured by placing a cuff and inflating it to block the blood flow. However, in face measurement, it is difficult to measure $T_2$. Thus, as a preliminary test, $T_2$ in the forearm was measured by placing a cuff on the upper arm and inflating it to 300-mm Hg to block the blood flow for 1 min. The results indicated that $T_2$ levels are relatively constant with few individual differences. In addition, similar findings of $T_2$ in a cat's cerebral cortex have been reported[20]. Despite a few measurement errors, facial SBF

seems to be inversely proportional to the slope of the thermal clearance curve, $\frac{d\log_e T_1(t)}{dt}$.

### 2.6.2 Participants and measurement conditions

A total of 132 healthy females in their 20s to 60s (those in their 20s ($26.2 \pm 0.50$ years of age, n = 36); those in their 30s ($31.6 \pm 0.18$ years of age, n = 22); those in their 40s ($46.2 \pm 0.42$ years of age, n = 43); those in their 50s ($50.6 \pm 0.28$ years of age, n = 11); and those in their 60s ($62.9 \pm 0.43$ years of age, n = 20)) were included in the main study. They were habituated for 30 min in the semi-supine posture at 25 °C and 50% RH, respectively.

From Eq. (3) derived from the TDM, the SBF was found to be inversely proportional to the slope of the thermal clearance curve. Thus, this study used the slope of the natural logarithm of skin temperature changes obtained in the main experiment as an index of the SBF. First, the cheek skin temperature and cheek SBF of the participants at rest were measured at a 50-cm distance for 5 min. Then, a far-infrared heater was used to apply a thermal load to the face for 30 s, and it was removed immediately after thermal loading to avoid the effects of radiation, conduction, and convection. Immediately afterward, the cheek skin temperature and cheek SBF were measured again for 5 min. The facial skin temperature was measured at 30 frames/s via thermography (TVS-700, NEC Avio Infrared Technologies, Tokyo, Japan). The facial SBF was measured using LSFG (30 frames/s, 2:1 interlace). Thermal loading was performed using a far-infrared heater (ERFT11KS, Daikin Industries, Osaka, Japan) with the temperature level set at 5.

### 2.6.3 Analysis

The slope of the natural logarithm of skin temperature changes during the 30 s after thermal loading was calculated by linear regression after resampling a $2.3 \times 3.0$ cm area of the participants' left cheek at a rate of 1 frame/s.

A mapping image was created according to the method described in Section 2.2. The analysis site was similar to that for TDM (ROI was $60 \times 80$ pixels). MBR was calculated from the mapping image obtained during a 30-s measurement after thermal loading.

### 2.7 Comparison Between SPG and LSFG

### 2.7.1 Overview of SPG

Strain-gauge plethysmography (SPG) (EC-5R, D. E. Hokanson, Washington, USA) is a method in which the venous occlusion cuff (compression band) is inflated to block the venous reflux by occluding the vein to detect the increase in fingertip volume (detecting the changes in the circumference of the fingertips as changes in impedance) owing to the influx of arterial blood with a strain gauge (at the center of the finger)[21]. This method allows the noninvasive intermittent measurement of the absolute values of the SBF

from fingertip volume changes, and its utility has been established[22].

Phase I is a change that occurs ~20 s immediately after venous occlusion when the venous return is 0; however, the influx of arterial blood is not inhibited. In other words, the increase in volume per unit time during a short duration accurately indicates the artery blood flow. Thus, when venous occlusion plethysmography is used, the blood flow can be measured correctly from the volume changes in phase I.

### 2.7.2 Participants and measurement conditions

Sixty healthy participants in their 20s, comprising 30 males ($23.3 \pm 0.39$ years of age) and 30 females ($23.8 \pm 0.49$ years of age), were habituated for 30 min in the semi-supine posture at 25 °C and 50% RH, respectively.

Figure 5(a) shows that in LSFG, noncontact measurements of the SBF of the third joint on the palm side of the middle finger of the nondominant hand placed on a desk 25 cm from the probe unit were performed. The measurements (30 frames/s, 2:1 interlace) were performed using an interval method in which the cycle of 5-s measurement, 10-s break, 5-s measurement, 10-s break, and 5-s measurement was repeated two times with a 3-min interval in between.

Figure 5(b) shows that the SPG measurement was performed by placing a sensor (strain gauge) on the third joint on the palm side of the middle finger of the nondominant hand and placing a cuff on the ipsilateral upper arm to measure SBF. After the calibration signal of 1% (1 ml/min/100 g tissue) was sent, the steady state at rest was measured for 15 s. Then, the vein of the measurement site was occluded by inflating the upper arm cuff to 50-mm Hg using a rapid cuff inflator (Biomedical Science Laboratory, Ishikawa, Japan). Then, 30 s later (when the arterial inflow curve of the measurement site became constant and the waveforms in the chart paper reached a plateau), the cuff was deflated, and 15 s later, the measurement was stopped. Then, the measurement was repeated after a 3-min interval.
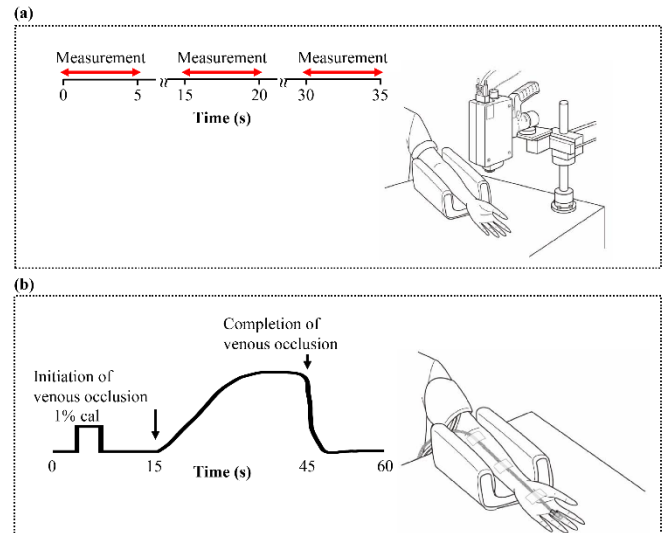


**Figure 5** Protocols of the LSFG method used in this study (a) and SBF measurements with SPG (conventional method) (b). The SBF measurements were performed on the third joint on the palm side of the middle finger of the nondominant hand. (a) LSFG measurement protocol: as demonstrated in method 2.7.2; (b) SPG measurement protocol: as demonstrated in method 2.7.2.

### 2.7.3 Analysis

A mapping image was created according to the method described in Section 2.2. The analysis site was around the third joint on the palm side of the middle finger of the nondominant hand (minor axis and major axis of elliptical area: $0.8 \times 1.6$ cm). MBR was calculated from the three measurements of 5-s mapping images.

In SPG, the intensity of the 1% calibration signal (1 ml/min/100 g tissue) was measured from a chart paper with a measure. The SBF of SPG was calculated from the slope of the tangent line drawn to the surge line of the pulse waves immediately after venous occlusion occurred.

## 2.8    Relationship Between SBF Index of LSFG and Age as well as Stratum Corneum Hydration

As a prototype application, the relationship between the blood flow index of the LSFG and aging as well as skin properties (stratum corneum hydration) was examined.

### 2.8.1 Participants and measurement conditions

Ninety-four healthy females ($43.6 \pm 14.4$ years of age) were included to study the relationship between the blood flow index of LSFG and aging. Forty healthy females ($30.1 \pm 2.01$ years of age) were included to study the relationship between the blood flow index of LSFG and stratum corneum hydration.

For LSFG measurement, subjects were habituated for 15 min in the semi-supine posture at 24 °C and 40% RH, respectively. Then, the SBF was measured from the front with the head fixed and the right cheek at 50-cm distance from the

probe unit. Continuous measurement (30 frames/s, 2:1 interlace) was performed for 30 s. For measuring stratum corneum hydration, the subjects were habituated for 15 min in the semi-supine posture at 20 °C and 40.0% RH, respectively. Measurements were performed by placing an impedance meter (SKICON-200EX, Yayoi Co., Tokyo, Japan) on the right cheek for a few seconds with constant pressure.

### 2.8.2 Analysis

A mapping image was created according to the method described in Section 2.2. Figure 3(e) shows that point 7), the ROI was the right cheek (i.e., an area defined by four vertices that have UV coordinates of (300, 200), (359, 219), (300, 269), and (359, 269)). From the mapping image obtained during a 30-s measurement, MBR was calculated as a blood flow index. Equation (4) demonstrates the blowout time (BOT), an index that represents the persistence of high blood flow, can be calculated as the ratio of the full width at half maximum of the MBR to the duration of one cardiac cycle (i.e., ratio of half-width duration to the duration of one cardiac cycle)[23].

$$BOT = \frac{Half-value\ width\ of\ a\ beat}{Cardiac\ cycle} \times 100. \qquad (4)$$

The stratum corneum hydration was calculated as the mean of three values after omitting the maximum and minimum values of five measurements.

### 2.9 Statistical Analysis

IBM SPSS Statistics for Windows v.25.0 (IBM, NY, USA) was used for all statistical analyses. The correlation between the two variables was evaluated using Pearson's product–moment correlation coefficient. Then, a simple linear regression analysis (with coefficient of determination $R^2$) was performed to examine whether the variance of these independent variables ($x$) can be explained by the dependent variable ($y$). Furthermore, the overall significance of the regression analysis was examined using one-way repeated-measures ANOVA. The significance of the regression coefficient and intercept was examined using a t-test. In the reliability analysis, the Bland–Altman analysis[24,25] was used to evaluate absolute reliability, and the intraclass correlation coefficient (ICC (2, k)) was used to assess inter-rater

reliability. A significance level of 0.05, or lower, was used for all statistical analyses.

### 2.10 Ethical Approval

All experiments described in this study were approved by the Kao Corporation Ethics Committee (#2011-08-58). All study participants were provided with a sufficient explanation of the contents and methods of the study, and written informed consent was obtained from them before performing the study procedures. All clinical trials conformed to the Declaration of Helsinki.

## 3. Results

### 3.1 Repeatability of SBF measured at a constant distance and angle

The SBF measurement was performed seven times within approximately 5 min on the left cheek of the same subjects (n = 60) at 50 cm measurement distance from the front (at an angle of 0°). The results of these MBR were: mean = 678.4, standard deviation = 25.5, and variation coefficient = 3.9, which suggests sufficient repeatability.

### 3.2 Comparison of Uniformity of SBF Measured at Different Distances

Fig. 6(a) revealed a significant positive correlation ($r^2$ = 0.927) between the two measurement distances (i.e., 25 cm and 50 cm), suggesting that the MBRs of the same measurement site (i.e., right cheek) are equivalent.

### 3.3 Comparison of Uniformity of SBF Measured at Different Angles

The results of the preliminary test indicated that the variation coefficients of the MBR of the forehead were low (4.25 ± 0.05) in the range of −30 ° to 30° but high in the ranges of −45 ° to −35° (5.32 ± 0.02) and 35° to 45° (5.80 ± 0.07). In other words, if the measurement angle exceeds 35° (−35°) to the left from the front and exceeds 35° (35°) to the right, the variation coefficients of the MBR increase. Thus, we decided to use angle ranges of −30° to 0° and 0° to 30°.
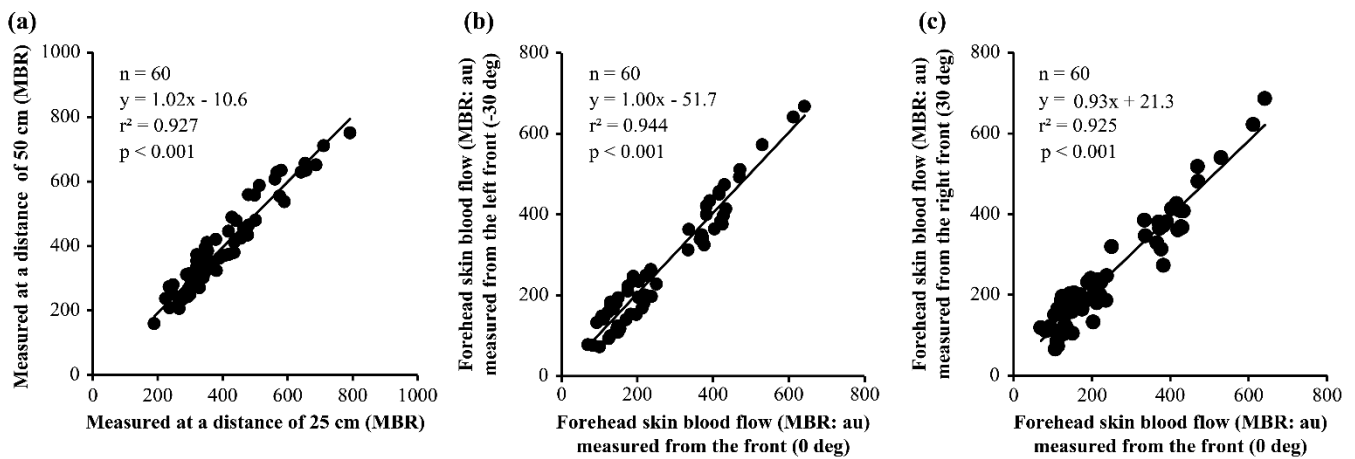
**Figure 6** Uniformity of the measurement of SBF at different measurement distances and angles.
(a) Comparison of MBR measured at distances of 50 and 25 cm in front of the right cheek; (b) comparison of MBR measured at a distance of 50 cm from the front (0°) and the left front (−30°) of the forehead; and (c) comparison of MBR measured at a distance of 50 cm from the front (0°) and the right front (30°).

Figures 6(b) and 6(c) show that there were significant positive correlations ($r^2 = 0.944$ and $r^2 = 0.925$, respectively) between the two measurement angle ranges (i.e., −30° to 0° and 0° to 30), suggesting that the MBRs of the same measurement site (i.e., forehead) are equivalent.

### 3.4 Comparison Between TDM and LSFG

The schematic in Fig. 7(a) reveals that the lower the facial SBF, the lower is the absolute value of the slope of the thermal clearance curve, and vice versa.

The scatter plot in Fig. 7(b) shows the relationship between (1) the slope of the thermal clearance curve (as an independent variable) measured using the already established TDM method (slope of natural logarithm of skin temperature changes after thermal loading) and (2) the MBR (as a dependent variable), an index of SBF determined by LSFG that is currently under development. The results suggest a linear relationship between the slope of the thermal clearance curve measured by TDM (*x*) and the MBR measured by LSFG (*y*). The slope of the line (−6634) and intercept (202) were determined by the least squares method. The coefficient of determination $R^2$ was 0.790, and the multiple correlation coefficient was 0.889. Thus, the results of the one-way repeated-measures ANOVA indicated the statistical significance of the coefficient of determination ($F > F_{0.001}$). In

addition, the results of the t-test indicated the statistical significance of the regression coefficient and intercept ($t > t_{0.001}$).

The results indicated a significant negative correlation between the slope of the thermal clearance curve and the MBR, suggesting MBR as an effective index of SBF.

### 3.5 Comparison Between SPG and LSFG

The scatter plot in Fig. 8 shows the relationship between (1) the SBF measured using the already established SPG method that allows the measurement of absolute SBF values and (2) the MBR (as a dependent variable), an index of SBF determined by LSFG that is currently under development. The results suggested a linear relationship between the SBF measured by SPG (*x*) and the MBR measured by LSFG (*y*). The slope of the line (42.2) and intercept (−14.7) were determined by the least squares method. The coefficient of determination $R^2$ was 0.980, and the multiple correlation coefficient was 0.990. Thus, the results of the one-way repeated-measures ANOVA indicated the statistical significance of the coefficient of determination ($F > F_{0.001}$). In addition, the results of the t-test indicated the statistical significance of the regression coefficient and intercept ($t > t_{0.005}$).
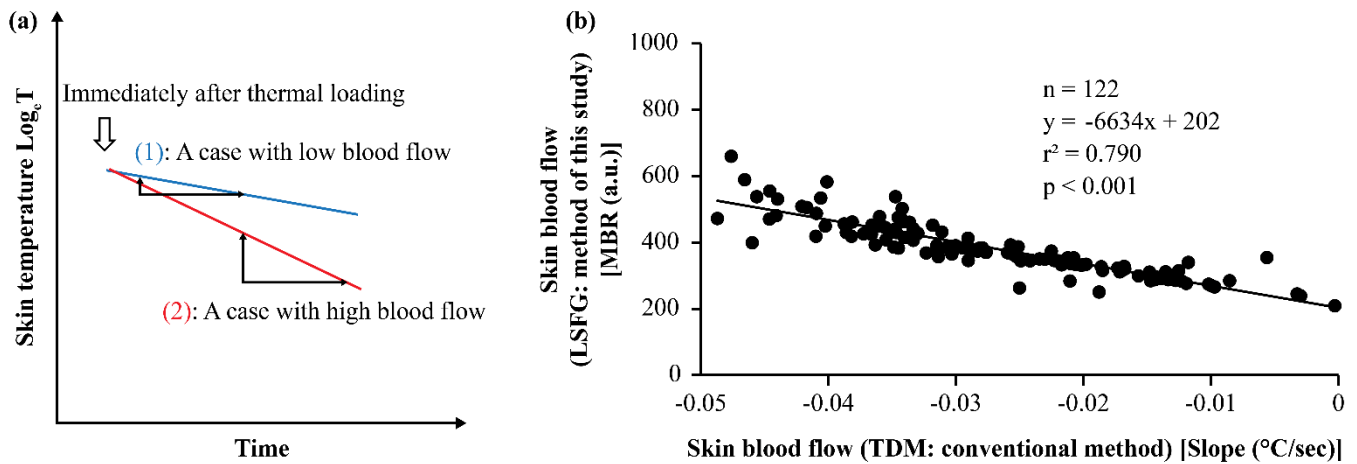
**Figure 7** Relationship between the slope of the thermal clearance curve in the TDM and the MBR.
(a) Typical example of facial SBF using TDM: (1) a case with low blood flow; (2) a case with high blood flow; and (b) a scatter plot showing the relationship between the slope of the thermal clearance curve measured using the TDM method (horizontal axis) and the MBR at rest determined by LSFG (vertical axis) in the right cheek.
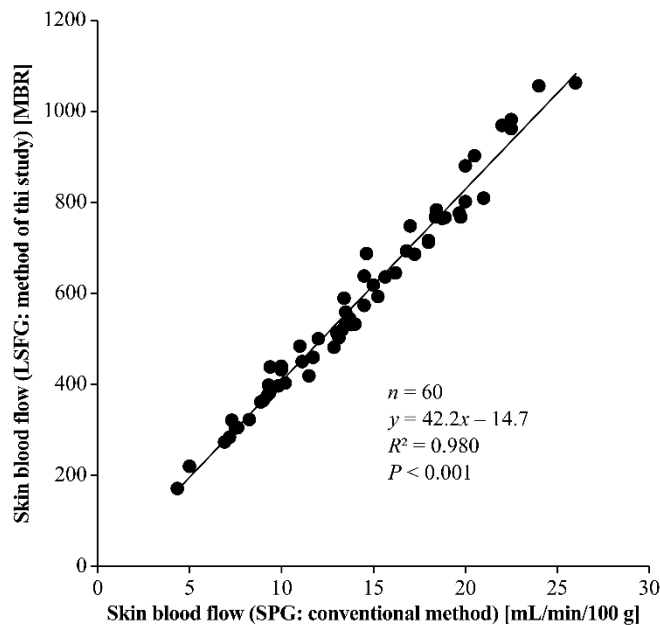


**Figure 8** Relationship between SBF measured using SPG and MBR. The SBF measurements were performed on the third joint on the palm side of the middle finger of the nondominant hand. A scatter plot showing the relationship between the SBF (ml/(min·100 g)) measured using SPG (horizontal axis) and MBR, which is an index of the LSFG (vertical axis).

The results indicated a significant positive correlation between the two measurement methods, suggesting that MBR determined by LSFG is an effective index of SBF. The experiment summary has been published in reference 26.

In SPG, the cuff is inflated to block the venous reflux by occluding the vein to measure the increase in the volume of the measurement site owing to the influx of arterial blood. Thus, the measurement site is limited to the limbs, preventing continuous measurement. In contrast, LSFG allows noninvasive and continuous measurement of SBF without limiting measurement area; thus, it is expected to have excellent clinical utility.

### 3.6 Bland–Altman analysis

Table 1 summarizes the Bland–Altman analysis results on the differences between measurements using various methods. Table 1(a) indicated that when reliability of SBF is compared between 25 cm and 50 cm, the 95% confidence interval of the mean difference between the two measurements (B–A) is distributed around 0, and well-balanced data is distributed above and below 0 on the y-axis ($-14.1$–$6.1$ (au)), which suggests that there is no fixed bias. The regression coefficient (RC) 0.055, which corresponds to the slope of the regression line, was not statistically significant (p = 0.128), which suggests the absence of proportional bias as well, such that the 5% limits of agreement (LOA) was $-81.3$–$73.3$ (au). Table 1(b) compares the SBF reliability measured at 0° to $-30$° and at 0° to 30°. The results suggested a fixed bias and proportional bias, and LOA was $-64.3$–$72.4$ (au) and $-72.6$–$81.5$ (au). Table 1(c) compares the reliability of SBF between TDM and LSFG, and it suggested a fixed bias and proportional bias, and LOA was $-89 \times 10^{-4}$–$101 \times 10^{-4}$ (°C/s). Table 1(d) compares the reliability of SBF between SPG and LSFG, and it suggests the presence of fixed and proportional biases, where LOA was $-1.51$–$1.51$ (ml/(min·100 g)).

**Table 1** Results of Bland–Altman analysis on the measurements of various methods (a, b, c, d)

| | N[*1] | Mean | SD[*2] | LOA[*3] | Fixed bias 95%CI[*4] | Proportional bias RC[*5] | P-value |
|---|---|---|---|---|---|---|---|
| | | | | | | Proportional bias | |
| | | | | | 95%CI[*4] | RC[*5] | P-value |
| **(a) Comparison of different distances** | | | | | | | |
| A. Measured at 25 cm distance [au][*6] | | 402.2 | 138.0 | | | | |
| B. Measured at 50 cm distance [au] | | 398.2 | 145.7 | | | | |
| Mean of measurements at A and B $\left(\frac{A+B}{2}\right)$ [au] | 60 | 400.2 | 145.7 | -81.3 ~ 73.3 | -14.1 ~ 6.1 | 0.055 | 0.128 |
| Difference of measurements at A and B (B-A) [au] | | -4.0 | 39.4 | | | | |
| **(b) Comparison of different angles** | | | | | | | |
| C. Measured angle 0°[au] | | 254.7 | 143.9 | | | | |
| D. Measured angle -30°[au] | | 258.8 | 147.7 | | | | |
| E. Measured angle 30°[au] | | 259.2 | 139.7 | | | | |
| Mean of measurements at C and D $\left(\frac{C+D}{2}\right)$[au] | 60 | 256.8 | 144.8 | -64.3 ~ 72.4 | -4.9 ~ 13.0 | 0.027 | 0.396 |
| Difference of measurements at C and D (D-C) [au] | | 4.0 | 34.9 | | | | |
| Mean of measurements at C and E $\left(\frac{C+E}{2}\right)$[au] | | 257.0 | 140.4 | -72.6 ~ 81.5 | -5.6 ~ 14.5 | -0.030 | 0.406 |
| Difference of measurements at C and E (E-C) [au] | | 4.4 | 39.3 | | | | |
| **(c) Comparison between TDM and LSFG of techniques** | | | | | | | |
| F. TDM[*7] (°C/sec) | | $-272 \times 10^{-4}$ | $109 \times 10^{-4}$ | | | | |
| G. LSFG[*8] (°C/sec) | | $-266 \times 10^{-4}$ | $112 \times 10^{-4}$ | | | | |
| Mean of measurements at F and G $\left(\frac{F+G}{2}\right)$ (°C/sec) | 122 | $-269 \times 10^{-4}$ | $107 \times 10^{-4}$ | -89 ~ 101 $(\times 10^{-4})$ | -3 ~ 14 $(\times 10^{-4})$ | 0.029 | 0.230 |
| Difference of measurements at F and G (G-F) (°C/sec) | | $6 \times 10^{-4}$ | $49 \times 10^{-4}$ | | | | |

Journal **XX** (XXXX) XXXXXX     Author *et al*

**(d) Comparison between SPG and LSFG of devices**

| | | | | | | | |
|---|---|---|---|---|---|---|---|
| H. SPG[*9] [ml/(min·100 g)] | | 14.1 | 5.06 | | | | |
| I. LSFG [ml/(min·100 g)] | | 14.1 | 5.11 | | | | |
| Mean of measurements at H and I $\left(\frac{H+I}{2}\right)$ [ml/(min·100 g)] | 60 | 14.1 | 5.07 | -1.51 ~ 1.51 | -0.20 ~ 0.20 | 0.012 | 0.564 |
| Difference of measurements at H and I (I-H) [ml/(min·100 g)] | | $1 \times 10^{-4}$ | 0.77 | | | | |

Abbreviations, *1: number of samples, *2: standard deviation, *3: 95% limits of agreement, *4: 95% coefficient interval, *5: regression coefficient *6: arbitrary unit, *7: thermal diffusion method, *8: laser speckle flowgraphy, *9: strain-gauge plethysmography

### 3.7 Intra-class correlation coefficient analysis

The intra-class correlation coefficient (ICC) of Case 2: ICC (2, K) was used to statistically analyze inter-tester reliability. Measurements were taken at two sites—1) the forehead and 7) right cheek—as shown in Fig. 4(e). Testers were five researchers who measured facial SBF four times each on sites 1) and 7) on 10 subjects. The ICC was 0.998 on the forehead and cheek, indicating significant inter-tester reliability (p < 0.001).

### 3.8 Relationship Between SBF Index (BOT) of LSFG and Age as well as Stratum Corneum Hydration

The scatter plot in Fig. 9(b) shows the relationship between (1) age (as an independent variable) and (2) the BOT (arbitrary unit), an index that represents the persistence of high blood flow as measured by LSFG (as a dependent variable). The results suggested a linear relationship between age ($x$) and BOT ($y$). The slope of the line ($-0.186$) and intercept (71.7) were determined by the least squares method. The coefficient of determination $R^2$ was 0.254, and the multiple correlation coefficient was 0.504. Thus, the one-way repeated-measures ANOVA indicated the statistical significance of the coefficient of determination ($F > F_{0.001}$). In addition, the t-test indicated the statistical significance of the regression coefficient and intercept ($t > t_{0.005}$). Thus, there was a significant negative correlation between the BOT and age.

The scatter plot in Fig. 9(c) shows the relationship between (1) the BOT (as an independent variable) and (2) the stratum corneum hydration (as a dependent variable). The results suggest a linear relationship between the BOT ($x$) and the stratum corneum hydration ($y$). The slope of the line (6.81) and intercept ($-186$) were determined by the least squares method. The coefficient of determination $R^2$ was 0.172, and the multiple correlation coefficient was 0.415. Thus, the results of the one-way repeated-measures ANOVA indicated the statistical significance of the coefficient of determination ($F > F_{0.01}$). In addition, the results of the t-test indicated the statistical significance of the regression coefficient and intercept ($t > t_{0.01}$). Thus, there was a significant positive correlation between the BOT and the stratum corneum hydration. Overall, the results indicated that the stratum corneum hydration is high when the SBF is high.
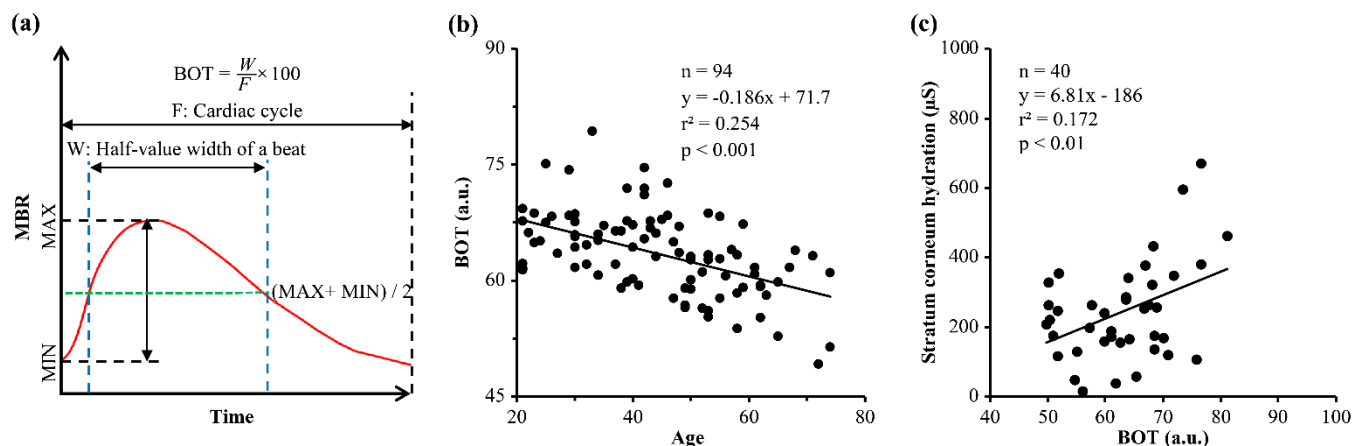


**Figure 9** Relationship between BOT (a) and age (b) and stratum corneum hydration (c).
(a) BOT (blowout time: an index that represents the persistence of high blood flow) can be calculated as the ratio of the full width at half maximum of the MBR to the duration of one cardiac cycle; (b) relationship between BOT of buccal blood flow and age; and (c) relationship between BOT of buccal blood flow and stratum corneum hydration.

## 4. Discussion

The stability of SBF measurement with LSFG is high because it uses a heartbeat map in which MBR, an index of blood flow, is normalized by defining one heartbeat as one cycle. In addition, facial mapping image, which was created by superimposing the heartbeat map image onto the video image based on the corresponding points, is useful in the analysis of regional blood flow because it clearly demonstrated the face boundary region.

In the seborrheic area of the face, the skin sometimes appears shiny owing to excess sebum. It is difficult to analyze the SBF in such a seborrheic area, as the specularly reflected light interferes with the light scattered by blood cells in subcutaneous vessels. The polarization direction of the incident light is preserved in the specularly reflected light. By contrast, because light scattered by blood cells in subcutaneous vessels is emitted after multiple instances of scattering in the skin, the polarization of the incident light is not preserved. Thus, each of the different polarized lights can

1
2
3
4
5
6
7
8
9
10
11
12
13
14
15
16
17
18
19
20
21
22
23
24
25
26
27
28
29
30
31
32
33
34
35
36
37
38
39
40
41
42
43
44
45
46
47
48
49
50
51
52
53
54
55
56
57
58
59
60

be used to extract the specularly reflected light and the light scattered by blood cells in subcutaneous vessels separately. The specularly reflected light was barely observed when the polarizing filter was placed in front of the probe unit and rotated by 90° (perpendicular to the direction parallel to the polarization direction of the surface-reflected laser light). Thus, when measuring the SBF in the seborrheic area using LSFG, the SBF can be analyzed effectively by reducing the specularly reflected light by placing the polarizing filter perpendicular to the polarization direction of the surface-reflected laser light.

### 4.1 Comparison of Uniformity of SBF Measured at Different Distances

In conventional laser speckle imaging, SBF is measured at a constant distance. Therefore, it is impossible to compare the SBF at the same site by increasing the magnification and reducing the measurement distance. However, in a clinical setting, by measuring the SBF of the entire face, it is desirable to understand the overall SBF before measuring the regional SBF to compare the two. Thus, we examined a method that allows a comparison of the uniformity of the SBF measured at different distances. Because the measurement of the SBF of the entire face is possible at 50-cm distance, this study was based on an MBR measurement distance of 50 cm. The following linear relationship is established between the velocity and the MBR:

$$MBR_{50} = MBR_{n,m,t} \times C_{50} + Offset_{50}, \qquad (5)$$
$$MBR_{25} = MBR_{n,m,t} \times C_{25} + Offset_{25}, \qquad (6)$$

When $MBR_{n,m,t}$ are provided in equation (2) and are the values of MBR in the nth and mth image for time t; $C_{50}$, a constant for the measurement distance of 50 cm; $C_{25}$, a constant for the measurement distance of 25 cm; $Offset_{50}$, the intercept for the measurement distance of 50 cm; and $Offset_{25}$, the intercept for the measurement distance of 25 cm.

When $MBR_{50} = MBR_{25}$,

$$MBR_{n,m,t} \times C_{50} + Offset_{50} = MBR_{n,m,t} \times C_{25} + Offset_{25}. \qquad (7)$$

By changing $MBR_{n,m,t}$, C and *Offset* can be calculated. The scatter plots in Fig. 6(a) were created based on Eqs. (5)–(7). Thus, it was suggested that the SBF measured at distances of 50 and 25 cm is equivalent[27].

### 4.2 Comparison of Uniformity of SBF Measured at Different Angles

In LSFG, the horizontal angle at a measurement distance of 50 cm was 24° (22 × 20 cm). In this study, the stability of the measurement of the forehead area of 0.9 × 1.8 cm (25 × 50

pixels) at a distance of 50 cm with measurement angle ranges of −30° (left front) to 0° (front) and 0° (front) to 30° (right front) was high. However, in the measurement of an uneven surface, such as the nose, eye corners, and edge of face, the measurement angle range may need to be reduced. This issue requires further investigation.

### 4.3 Comparison Between TDM and LSFG

The correlation between the TDM results presented in references [16–18] and LSFG was examined by synchronizing the scanning period of the cheek SBF in a 2D space. According to Grayson's theory (Grayson, 1952), there is a significant negative correlation between the slope of the thermal clearance curve and the SBF[19]. Thus, the results suggest that the MBR determined by LSFG is an effective index of the SBF.

### 4.4 Comparison Between SPG and LSFG

In SPG, the measurement site is limited to the limbs, and continuous measurement is not possible. The blood flow in the forearm is measured using SPG to calculate the sum of the muscle blood flow and SBF. This study used the fingers as the measurement site for SPG because the muscle components necessary for the extension and contraction of fingers are in the palms and forearms but not in the fingers[28,29]. Thus, the measurement of the blood flow in the fingers by SPG allows the measurement of the finger SBF only. The results indicated a significant positive correlation between LSFG and SPG, suggesting that the MBR determined using LSFG is an effective index of SBF. LSFG allows noninvasive and continuous measurement of the SBF without limiting the measurement area and is thus expected to have excellent clinical utility in the future.

### 4.5 Relationship Between SBF Index (BOT) of LSFG and Age as well as Stratum Corneum Hydration

#### 4.5.1 Relationship between BOT and age

Among studies that have used laser Doppler flowmetry to examine the relationship between aging and facial SBF, one study did not find significant age-related changes, probably because of a small sample size[30]. Another study found a significant age-related decrease in SBF in areas with relatively high SBF[31]. Furthermore, another study found an age-related decrease in the vasodilation response to thermal loading[32]. In addition, this study found an age-related decrease in the frequency of the vasoconstriction response to cooling loading[32]. In our previous study, which involved our integration-type laser Doppler flowmeter with a temperature-loading instrument[4], no significant age-related changes in the flow decrease rate (FDR) were observed. However, a significant age-related reduction in the slope of the SBF with time was found during cooling loading ($S_{fall}$). In addition, a

study that used the immunohistochemical method demonstrated a significant age-related decrease in SBF in photo-exposed areas[33]. In the present study, we found a significant negative correlation between age and the BOT (blowout time, an index that shows the persistence of high blood flow), suggesting an age-related decrease in the BOT. Because the BOT calculates the ratio of the full width at half maximum of the MBR to the duration of one cardiac cycle, thereby allowing comparisons between individuals, it is possible to examine age-related changes.

### 4.5.2 Relationship between BOT and stratum corneum hydration

Considering the moisture supply from the SBF to the stratum corneum, there may be a significant correlation between SBF and stratum corneum hydration. However, only a few studies have found a significant correlation between the two[31]. To reduce age-related effects, 40 healthy females (30.1 ± 2.01 years of age; age range: 27–33 years) were included in our study of the relationship between the BOT, a blood flow index of LSFG, and the stratum corneum hydration in the cheek area. The results indicated a significant positive correlation between the BOT and the stratum corneum hydration. The humidity of the external environment and moisturizing factors, such as natural moisturizing factors, intercellular lipid and sebum barrier, are a few of the factors besides SBF that may regulate stratum corneum hydration. Therefore, the correlation coefficients may seem comparatively low to the correlations between devices measuring the same factors. However, the results can be considered decent as correlations between two factors, given that the comparisons of biological factors between individuals comprise many variation factors. They suggest that the BOT, unlike conventional SBF indices, reflects the persistence of high SBF.

## 5. Conclusion

The conclusions of this study can be summarized as follows.
(1) The practicability of SBF measurement using LSFG is high because LSFG uses a heartbeat map in which MBR, an index of SBF, is normalized by defining one heartbeat as one cycle.
(2) Because mapping images clearly show the face boundary region, they are useful for the analysis of regional blood flow.
(3) By using a morphing technology with a face mesh to compare localized differences in facial SBF among individuals, the blood flow of the area proportional to the face size can be calculated.
(4) The SBFs measured at distances of 25 and 50 cm are equivalent.

(5) The practicability of SBF measurement at a 50 cm distance with a measurement angle range of −30° to 30° is high. Thus, this method is suitable for practical use.
(6) There was a significant negative correlation between the MBR and the slope of the thermal clearance curve (slope of natural logarithm of skin temperature changes after thermal loading) and the MBR. The results suggested that the MBR determined using LSFG is an effective index of SBF.
(7) There was a significant positive correlation between the SBF determined using SPG and MBR. The results suggested that MBR determined using LSFG is an effective index of SBF.
(8) There was a significant negative correlation between the BOT and age, suggesting an age-related decrease in the persistence of high SBF.
(9) The BOT exhibited a significant positive correlation with stratum corneum hydration.

Because the LSFG device can evaluate the SBF through noninvasive and continuous measurements without limiting the measurement area, the results suggest its high applicability for medicine and cosmetology.

## Disclosures

No conflicts of interest, financial or otherwise, are declared by the authors.

## Acknowledgments

## References

[1] Nagashima Y, Yada Y, Suzuki T and Sakai A 2003 *International Journal of Biometeorology* **47** 139-147
[2] Stern MD 1975 *Nature* **254** 56-58
[3] Nilsson GE, Tenland T and Oberg PA 1980 *IEEE Transactions on Biomedical Engineering* **27** 12-19
[4] Bonner RF, Clem TR, Bowen PD and Bowman RL 1981 in *Biological Applications in Scattering Techniques Applied to Supramolecular and Nonequilibrium Systems*, Chem SH, Ed., pp. 685-701, Springer, Boston
[5] Fercher AF and Briers JD 1981 *Optics Communication* **37** 326-330
[6] Wårdell K, Jakobsson A and Nilsson GE 1993 *IEEE Transactions on Biomedical Engineering* **40** 309-316
[7] Konishi N, Tokimoto Y, Kohra K, and Fujii H 2002 *Optical Review* **9** 163-9
[8] Fujii H, Nohira K, Yamamoto Y, Ikawa H and Ohura T 1987 *Applied Optics* **26** 5321-5

Author *et al*

[9]     Goodman JW 1975 in *Laser Speckle and Related Phenomena (Section 2.6), Topics in Applied Physics* **9**, Dainty JC Ed., 46-60, Springer-Verlag Berlin Heidelberg, New York

[10]   Philipp M and Philipp G 2009 Advances in geometric morphometrics *Evolutionary Biology* **36** 235-247

[11]   Miyashita W and Nakahara R 2005 Three-dimensional average faces in Japanese with normal occlusion-Evaluation of construction method and reproducibility *Orthodonthic Waves-Japan Ed.* **64** 36-43

[12]   Tamaki Y, Araie M, Tomita K, Nakahara M, Tomidokoro A and Fujii H 1997 *Japan Journal Ophthalmology* **41** 49-54

[13]   Lee MC, Konishi N and Fujii H 2003 *Optical Review* **10** 562-566

[14]   Anderson RR 1991 *Archives of Dermatology* **127** 1000-1005

[15]   Groner W, Winkelman JW, Harris AG, Ince C, Bouma GJ, Messmer K and Nadeau RG 1999 *Nature Medicine* **5**(10) 1209

[16]   Aschoff J and Wever R 1957 *Verh Dtsch Ges Kreislaufforsch* **23** 375-380

[17]   Schroder J and Voridis J 1955 *Pflugers Archiv fur die gesamte Physiologie des Menschen und der Tiere* **261** 550-556

[18]   Sakai A 1988 *Japanese Journal of Applied Physiology* **18** 5-10

[19]   Grayson J 1952 *Journal of Physiology* **118** 54-75

[20]   Philip Carter L, Erspamer R and Bro WJ 1981 *Stroke* **12** 513-518

[21]   Hokanson DE, Sumner DS and Strandness DE 1975 *IEEE Transactions on Biomedical Engineering* **22** 25-29

[22]   Branten AJ, Smits P, Jansen TT, Wollersheim H and Thien T 1996 *Journal of Cardiovascular Pharmacology* **27** 303-306

[23]   Shiba T, Takahashi M, Hashimoto R, Matsumoto T and Hori Y 2016 *Graefe's Archive for Clinical and Experimental Ophthalmology* **254** 1195-1200

[24]   Bland JM and Altman DG 1986 *Lancet* **i** 307-310

[25]   Bland JM and Altman DG 1995 *Lancet* **346** 1085-1087

[26]   Nagashima Y, Ohsugi Y, Niki Y, Maeda K and Okamoto T 2015 *Proceedings of SPIE* **9792**, 979218

[27]   Nagahara M, Tamaki Y, Tomidokoro A and Araie M 2011 *Investigative Ophthalmology & Visual Science* **52** 87-92

[28]   Agur AMR and Dalley AF 2017 Upper limb in *Grant's Atlas of Anatomy* (Chapter 2), 14th Ed., pp. 140-163, Wolters Kluwer, Alphen aan den Rijn, Netherlands

[29]   Birch R 2015 Pectoral girdle and upper limb in *Gray's Anatomy* (Section 6), 41st Ed., S. Standring, Ed., pp. 879-885, Elsevier, Amsterdam, Netherlands

[30]   Kelly RI, Pearse R, Bull RH, Leveque JL, de Rigal J and Mortimer PS 1995 *Journal of the American Academy of Dermatology* **33** 749-756

[31]   Ishihara M et al. 1988 Cutaneous Blood flow in *Cutaneous Aging*, A. M. Kligman, Y. Takase, Eds., pp. 167-181, University of Tokyo Press, Tokyo

[32]   Tolino MA and Wilkin JK 1988 *In Journal of Investigative Dermatology* **90**, 613

[33]   Chung JH, Yano K, Lee MK, Youn CS, Seo JY, Kim KH, Cho KH, Eun HC Detmar M 2002 *Archives of Dermatology* **138**, 1437-1442